Experimental and Numerical Study for the Shear Strengthening of RC Beams Using Textile Reinforced Mortar

Yousef A. Al-Salloum[1]; Hussein M. Elsanadedy[2]; Saleh H. Alsayed[3]; and Rizwan A. Iqbal[4]

Abstract: In this paper, the effectiveness of textile-reinforced mortars (TRM), as a means of increasing the shear resistance of reinforced concrete beams, is experimentally and numerically investigated. Textiles comprise of fabric meshes made of long woven, knitted or even unwoven fiber rovings in at least two (typically orthogonal) directions. Mortars—serving as binders—may (or may not) contain polymeric additives usually used to have improved strength properties. These TRM may be considered as an alternative to fiber reinforced polymers (FRP), providing solutions to many of the problems associated with application of the latter without compromising much of the performance of strengthened members. In the present study, a new type of textile (basalt-based textile) was used as strengthening material. Two different mortar types' viz. cementitious and polymer-modified cementitious mortars were used as binding material for the textile sheets. The studied parameters also included the number of textile layers as well as the orientation of the textile material. The experimental program comprises of testing two control beams which were intentionally designed to be deficient in shear, in addition to testing eight beams which were externally upgraded by TRM sheets for enhancing their shear capacity. On the basis of the experimental response of reinforced concrete members strengthened in shear, it is concluded that textile-mortar composite provides substantial gain in shear resistance; this gain is higher as the number of layers increases. With higher number of layers, textile with 45° orientation along with polymer-modified cementitious mortar provides the highest shear strength enhancement. Nonlinear finite element (FE) analysis was also carried out on the tested beams using LS-DYNA, which is transient nonlinear dynamic analysis software. The numerical analysis carried out involved case studies for TRM modeled, with and without mortar. Good agreement was achieved between the experimental and numerical results especially for the ultimate load carrying capacity for the case of FE models incorporating mortar. The study was extended numerically to include additional cases of TRM-strengthened specimens with more number of TRM layers as well as a case of FRP-strengthened specimen. **DOI: 10.1061/(ASCE)CC.1943-5614.0000239.**

CE Database subject headings: Mortars; Concrete beams; Shear strength; Finite element method; Experimentation; Fiber reinforced materials.

Author keywords: Textile reinforced mortar; Concrete beams; Shear strengthening; Finite element modeling.

Introduction

The call for rehabilitating existing structures has been so frequent in the past years because of deterioration and/or the introduction of more strict design requirements. One of the most common upgrading techniques for reinforced concrete members involves the use of fiber reinforced polymer (FRP) jackets, which are aimed at increasing the shear resistance in regions with inadequate transverse reinforcement. The use of FRP has gained increasing popularity in the civil engineering community, because of the favorable properties possessed by these materials, namely: extremely high strength-to-weight ratio, corrosion resistance, ease and speed of application, and minimal change in the geometry (fib bulletin 2001). Despite all these advantages, the FRP strengthening technique has a few disadvantages, which are attributed to the resins used to bind or impregnate the fibers (Triantafillou et al. 2006; Papanicolaou et al. 2008; Triantafillou and Papanicolaou 2006). These drawbacks may include: (a) debonding of FRP from the concrete substrate; (b) poor behavior of epoxy resins at temperatures above the glass transition temperature; (c) relatively high cost of epoxies; (d) inability to apply FRP on wet surfaces or at low temperatures; (e) lack of vapor permeability, which may cause damage to the concrete structure; (f) incompatibility of epoxy resins and substrate materials; and (g) difficulty to conduct postearthquake assessment of the damage suffered by the reinforced concrete behind (undamaged) FRP jackets. One possible solution to the previously listed problems would be the replacement of organic with inorganic binders, e.g., cement-based mortars, leading to the replacement of FRP with fiber reinforced mortars (FRM). As a consequence of the granularity of the mortar, penetration and impregnation of fiber sheets is very difficult to achieve; also, unlike resins, mortars cannot wet individual fibers.

Despite the bond-related problems, the use of composites with inorganic matrices in the field of structural upgrading has not escaped the attention of the research community. The performance of carbon fiber sheets with an inorganic matrix made of

[1]Professor, Dept. of Civil Engineering, King Saud Univ., Riyadh 11421 (corresponding author), E-mail: ysalloum@ksu.edu.sa.Saudi Arabia.

[2]Assistant Professor, Dept. of Civil Engineering, King Saud Univ., Riyadh 11421, Saudi Arabia.

[3]Professor, Dept. of Civil Engineering, King Saud Univ., Riyadh 11421, Saudi Arabia.

[4]Research Assistant, Dept. of Civil Engineering, King Saud Univ., Riyadh 11421, Saudi Arabia.

Note. This manuscript was submitted on January 24, 2011; approved on June 14, 2011; published online on June 16, 2011. Discussion period open until July 1, 2012; separate discussions must be submitted for individual papers. This paper is part of the ***Journal of Composites for Construction***, Vol. 16, No. 1, February 1, 2012. ©ASCE, ISSN 1090-0268/2012/1-0–0/ $25.00.

aluminosilicate powder and a water-based activator has been evaluated by Kurtz and Balaguru (2001) and Garon et al. (2001). These materials were used as externally bonded flexural strengthening reinforcement of concrete beams (Kurtz and Balaguru 2001) or plain concrete prisms (Garon et al. 2001) and resulted in comparable performance with epoxy-impregnated sheets in terms of strength and stiffness, with some reduction in ductility. The fatigue performance of concrete beams strengthened in flexure with carbon fiber sheets bonded with the same inorganic matrix was evaluated by Toutanji et al. (2003), and was found satisfactory. Large-scale tests conducted on concrete beams strengthened in flexure or shear with externally bonded carbon sheets in a polymer-modified cementitious matrix have demonstrated that the technique is promising (Wiberg 2003). In one study (Wu and Teng 2003), unidirectional carbon sheets bonded with a cementitious binder were employed to confine small (100×200 mm) cylinders. Confined specimens in this study exhibited high strength and sufficient deformability, comparable to that of companion specimens wrapped with epoxy-impregnated carbon sheets.

Bond conditions in cementitious composites could be improved and fiber-matrix interactions could be made tighter when continuous fiber sheets are replaced by textiles (Papanicolaou et al. 2008). These materials comprise fabric meshes made of long woven, knitted or even unwoven fiber rovings in at least two (typically orthogonal) directions. The density, that is the quantity, and the spacing of rovings in each direction can be controlled independently, thus, affecting the mechanical characteristics of the textile and the degree of penetration of the mortar matrix through the mesh. A literature review of studies on the use of textiles in the upgrading of concrete structures has revealed the following: the work reported in Curbach and Ortlepp (2003) focused mainly on the bond between concrete and cement-based textile composites; the work in Curbach and Brueckner (2003) presents test results on RC beams strengthened with two or three layers of alkaline resistant (AR) glass textile combined with cementitious mortar; and the work reported in Triantafillou et al. (2006) demonstrates the effectiveness of cement-based textile composites in the form of jackets to confine concrete in compression.

In a recent study, Larbi et al. (2010) studied the mechanical feasibility of textile-reinforced concrete plate for strengthening of RC beams by comparing them with traditional solutions such as (CFRP). Three distinct mortar-based composite mixes (hydraulic mortar associate with glass grid and glass mat, inorganic phosphate cement associate with glass mat, and ultrahigh mortar performances combined with short metallic fibers) and two strengthening shapes were used—the U reinforcement and the side reinforcement—and compared with CFRP results. The experimental study comprised of testing beams under three-point bending tests and measuring displacement at the midspan and the strains in the transverse bars near the support. It was concluded on the basis of the results from the study that, quantitatively the CFRP and the textile-reinforced mortar materials have similar behavior, especially in the final stage. Also, the Ritter-Morsch truss model can be accurately used for the evaluation of tensile strength of beams strengthened by textile-reinforced mortars (TRM) material. The results of the study indicate that a significant increase in the carrying capacity and bending stiffness was obtained by the use of mortar-based composite material. The U-shaped reinforced beams were found to be effective for the three used reinforcements. The side surface reinforced beam with ultrahigh performance mortar-shirt metallic fibers presented performances closer to the CFRP-strengthened beams, as long as the anchorage is of sufficient length.

In a research study by Papanicolaou et al. (2008), the performance of textile-reinforced mortar in comparison with FRPs as strengthening material of unreinforced masonry walls subjected to cyclic out-of-plane loading, was experimentally investigated. The results from the study concluded that TRM jacketing provided substantial increase in strength and deformability. It was seen that compared with the epoxy-based polymers, the TRM may even result in higher effectiveness. The study concluded that TRMs could be an extremely promising solution for structural upgrading of masonry structures under out-of-plane loading. Near surface mounted (NSM) overlays were also considered as reinforcement and the performance of the masonry walls during the tests suggested that NSM reinforcement is less effective in strength but more effective in deformability compared to both TRM and FRP reinforcements.

Triantafillou and Papanicolaou (2006) investigated experimentally the effectiveness of TRM jackets for the shear strengthening of reinforced concrete members. The test matrix comprised of testing six beams designed to be deficient in shear in four-point bending. The parameters considered in the study included the use of mortar versus resin-based matrix material for the textile reinforcement, the number of layers, and the use of conventional wrapping versus spirally applied textiles. Four specimens were tested monotonically whereas the other two beams were tested by applying a load in a quasi-static cyclic pattern. On the basis of the results of the study, it was concluded that the closed-type textile-reinforced mortar jackets provide substantial gain in the shear capacity of the reinforced concrete members. Two layers of TRM reinforcement for both the conventional jackets as well as the spiral strips were sufficient to increase the shear capacity of the beams by more than 60 kN. One layer of textile reinforcement was sufficient to increase the shear capacity of the beam by 40 kN. However, a single layer of TRM reinforcement was only about 55% as effective as the resin-based FRP reinforcement. The study also concluded that the modeling of TRM jackets is as straightforward as the FRP jacketing through the introduction of experimentally derived jacket effectiveness coefficients which, however, require extensive experimental testing.

In a research paper, Wu and Sun (2005) reported findings from their project aimed at developing cement-based composite thin sheet for structural retrofit. They also compared the retrofit efficiencies of epoxy-based and cement-based thin sheets. Experimental tests in their study included compressive and flexural tests carried out on retrofitted concrete cylinders and beams. Cement-based matrix and epoxy resin were used separately to make thin carbon fiber reinforced cement (CFRC) and CFRP sheets. On the basis of the results of the study, it was concluded that the flexural and compressive strength of concrete can be significantly improved using external fiber reinforced cement (FRC) wraps. The ductility of the retrofitted concrete is also increased. The final failure of the confined concrete cylinder and the beam was much less explosive compared with the CFRP specimens. The difference between the compressive strength of concrete cylinders wrapped with CFRC and CFRP was negligible, however, the CFRP beam had a much higher flexural strength than the CFRC beam.

Test results from a study by Bruckner et al. (2008) indicate that thin layers of concrete utilizing textile reinforcement can be used as shear strengthening for reinforced concrete T-beams thereby increasing the shear capacity of these beams. The shear strengthening provided by textile-reinforced cement (TRC) was tested on T-beams designed deficient in shear. An anchoring system was also designed to sufficiently evaluate the bond anchoring outside of the compression zone. On the basis of the test results, it was concluded that the shear load carrying capacity of T-beams can be noticeably increased by applying TRC strengthening layers. However, the increase is only limited without the use of any mechanical anchoring of the strengthening layer.

Di Ludovico et al. (2010) studied the confinement effectiveness of basalt-based textile fibers bonded with cement-based matrix on concrete cylinders compared with glass fiber reinforced polymer (GFRP) laminates, alkali resistant fiberglass grids, and cement-based mortar alone. The experimental program consisted of testing 23 low concrete compressive strength cylinders after different curing times. The conclusions from the study indicate that the basalt reinforced mortar (BRM) could provide a substantial gain in both the compressive strength and the ductility of concrete members. It also resulted in a less brittle failure compared with the GFRP-wrapped specimens. It was finally concluded in the study that BRM technique seems an extremely promising solution to overcome the limitations of epoxy-based FRP laminates.

In the present study, a new type of textile (basalt-based textile) was used to strengthen reinforced concrete beam specimens to increase their shear capacity. Two different mortar types' viz. cementitious and polymer-modified cementitious mortars were used as binding material for the textile sheets. The studied parameters also included the number of textile layers as well as the orientation of the textile material. Finally, a numerical investigation utilizing nonlinear finite element analysis was carried out and a comparison was made between the experimental and numerical results. On the basis of the validation of results, the numerical study was expanded to include additional cases to study the shear enhancement of beams using more TRM layers, and a comparison with CFRP-strengthened beam specimen was made.

Experimental Program

Test Matrix

This study comprises of testing 10 simply supported small-scale RC beams (150 × 200 × 1500 mm) in four-point bending when externally upgraded by TRM sheets. The criterion for selection of the beam dimensions was on the basis of available resources in the laboratory. The goal is to study the effectiveness of TRM in enhancing the shear capacity of RC beams. The studied parameters included: type of mortar (cementitious versus polymer-modified cementitious), number of TRM layers, and textile orientation in the shear-span region. The test matrix is shown in Table 1. The test matrix has two control beams which were intentionally designed to be deficient in shear. These beams represent the worst case scenario of typical construction practices used earlier within the region of Saudi Arabia. Furthermore, the absence of shear reinforcement within the shear-span may represent the case of corroded shear stirrups as a result of harsh environmental conditions prevailing in the Kingdom of Saudi Arabia. Four beams were strengthened with textile-reinforced cementitious mortar; whereas, the last four beams were strengthened with polymer-modified cementitious mortar. Details of test beams are displayed in Fig. 1.

Properties of Materials

Concrete and Steel Reinforcement

Ready-mix concrete with a target compressive strength of 20 MPa was used to cast the beam specimens. Three standard cylinders (150 × 300 mm) were also cast which were tested under compression at 28 days as per the ASTM C39/39M standard (ASTM 2010). To determine the actual characteristics of steel reinforcement, five samples of steel bars for each diameter were tested under tension as per ASTM E8/E8M test standard (ASTM 2009). The average values for yield and tensile strengths of the bars are listed in Table 2. After the curing period for the concrete beams, the specimens, which were to be strengthened, were thoroughly sandblasted to remove dirt and any loose material. This was done to ensure optimum bond quality in between the concrete substrate and the TRM layers. Markings were made on the specimens to outline the TRM edges.

Textile-Reinforced Mortar

Two commercially available repair mortars (cementitious and polymer-modified cementitious) were utilized in this study. To determine the compressive strength of mortar, 50-mm cubes were prepared and then tested in accordance with ASTM C109 / C109M (ASTM 2008). For measuring the tensile strength of mortar, briquette specimens were prepared for each mortar type and tested in accordance with ASTM C190 (ASTM 1985). The measured properties of the two types of mortar used in this research are illustrated in Table 3.

Basalt-based textile, as shown in Fig. 2, was used in this study. To obtain the mechanical properties of the textile used, five nonstandard coupons of the bare textile were prepared and then tested in uniaxial tension (see Fig. 3). Table 4 presents the measured mechanical properties of the bare textile.

In addition to tests on mortar and bare textile, tests were carried out on TRM coupons to measure tensile properties as well as bond strength between the TRM and the concrete substrate. Nonstandard TRM tensile coupons were prepared for each mortar type using one layer of the basalt textile; at least five specimens were prepared of the dimensions given in Fig. 4(a) and then tested under uniaxial tension till failure. In addition, standard pull-out tests in accordance with ASTM D4541 (ASTM 2009) as shown in Fig. 4(b) were carried out on TRM specimens, adhered to an existing concrete substrate. Results of tension and pull-out tests are summarized in Table 5.

Table 1. Test Matrix

Specimen identification	Mortar type	Number of TRM layers each side	Textile orientation within shear-span (°)	Number of specimens
BS1		Control specimen		2
BS2	Cementitious	2	0/90	1
BS3	Cementitious	2	45/ − 45	1
BS4	Cementitious	4	0/90	1
BS5	Cementitious	4	45/ − 45	1
BS6	Polymer-modified cementitious	2	0/90	1
BS7	Polymer-modified cementitious	2	45/ − 45	1
BS8	Polymer-modified cementitious	4	0/90	1
BS9	Polymer-modified cementitious	4	45/ − 45	1
Total number of specimens				10

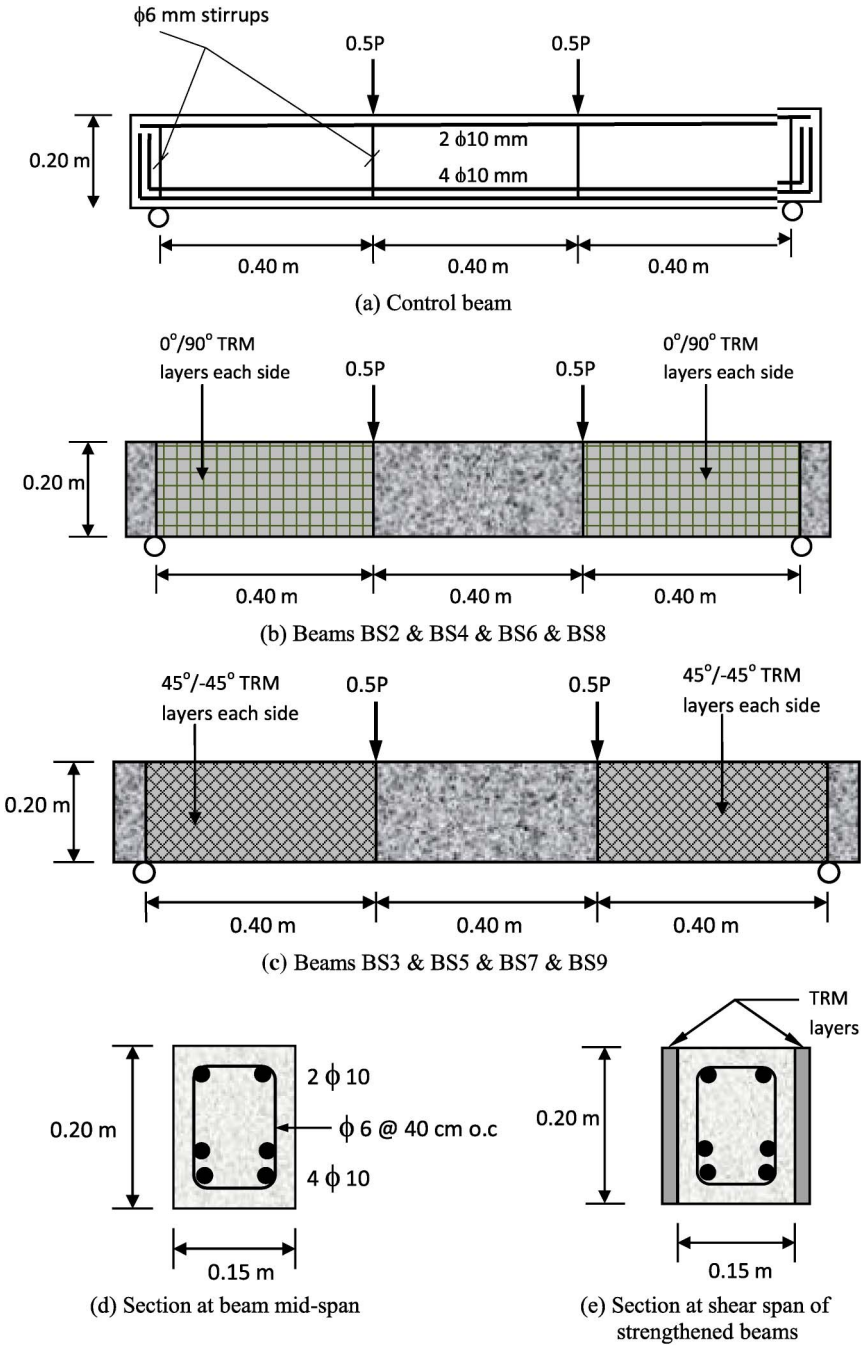

Fig. 1. Details of test beams

Table 2. Properties of Ø10- and Ø6 – mm Bars Used as Beam Reinforcement

Ø10 – mm bars		Ø6 – mm bars	
Tensile strength	Yield strength	Tensile strength	Yield strength
684 MPa	578 MPa	372 MPa	280 MPa

Table 3. Mechanical Properties of Mortars Used in This Study

Type	28-day tensile strength (MPa)	28-day compressive strength (MPa)
Cementitious mortar	2.77	23.9
Polymer-modified cementitious mortar	3.4	56.4

For TRM-strengthened specimens, a layer of mortar about 2 mm thick was applied on the beam specimens first using a metal trowel. The textile was then pressed slightly into the mortar until the mortar protruded out of the perforations between the rovings. The second mortar layer was then applied to completely cover the textile fabric and the procedure was repeated for each layer of TRM. Care should be taken, that the application process for each layer is done prior to the previous layer becoming dry.

Test Setup

The 10 beams were subjected to four-point bending at a total span of 1.20 m and a shear-span of 0.4 m. The load was applied using a stiff steel beam connected to 2000-kN AMSLER testing machine. A load cell was mounted between the machine and the rigid beam as shown in Fig. 5 to record load during the experiment.

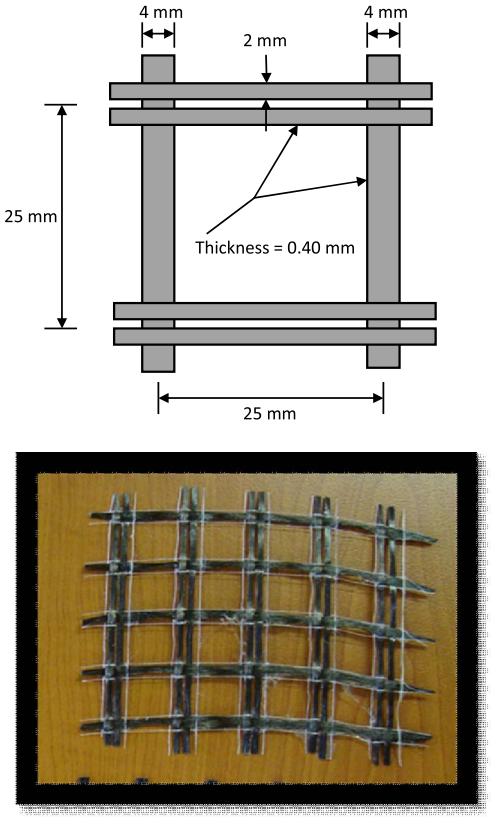

Fig. 2. Typical textile used in this study

(a) Before testing

(b) After testing

Fig. 3. Nonstandard bare textile coupons

Table 4. Mechanical Properties of Bare Basalt Textile Used in This Study

Source	Tensile strength (MPa)	Elastic modulus (GPa)	Nominal thickness per layer[a] (mm)
Laboratory	623	31.94	0.064

[a]On the basis of equivalent smeared distribution of bare textile fibers.

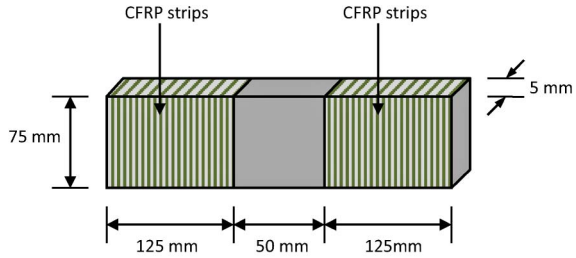

(a) Tensile coupons

(b) Pull-out test

Fig. 4. TRM test coupons

Table 5. Mechanical Properties of TRM Coupons

Mortar type	Tensile strength (MPa)	Ultimate tensile strain	Bond strength (MPa)
Cementitious mortar	7.7	0.0299	0.39
Polymer-modifiedcementitious mortar	8.23	0.0536	0.70

All specimens were monotonically loaded at a displacement rate of 1 mm/ min till failure. Three LVDTs were affixed underneath the beams to measure their deflections during the test. Moreover, strain gages were used to record strains at the level of steel reinforcement during the experiment. The sensor locations are shown in Fig. 5.

Test Results and Discussion

A summary of test results for all beams is displayed in Table 6. Load versus midspan deflection curves are presented as shown in Figs. 6 and 7 for beams with cementitious and polymer-modified cementitious mortars, respectively. In addition, final modes of failure are illustrated in Fig. 8 for representative samples of test beams. The two control beams (BS1-1 and BS1-2) failed in shear-compression mode, as expected, through the formation of diagonal cracks in the shear-span followed by concrete crushing

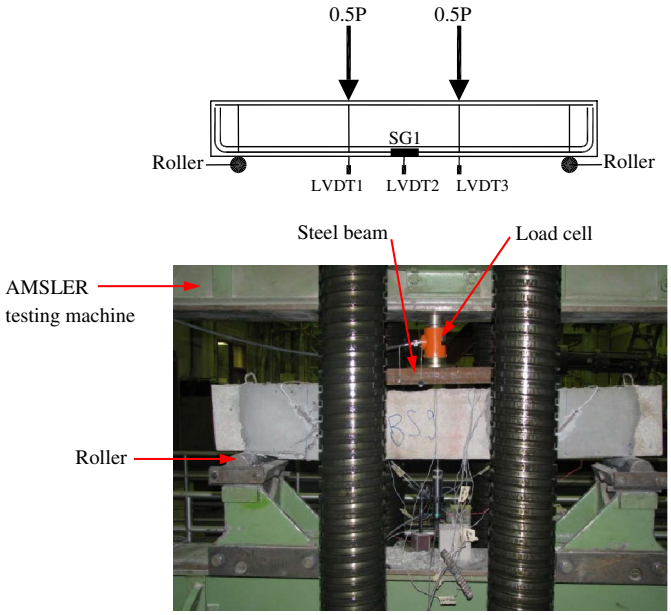

Fig. 5. Test setup and instrumentation

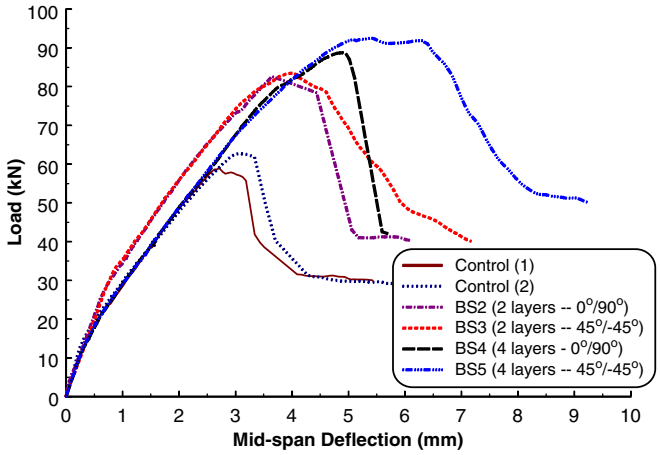

Fig. 6. Load-deflection curves for beams with cementitious mortar

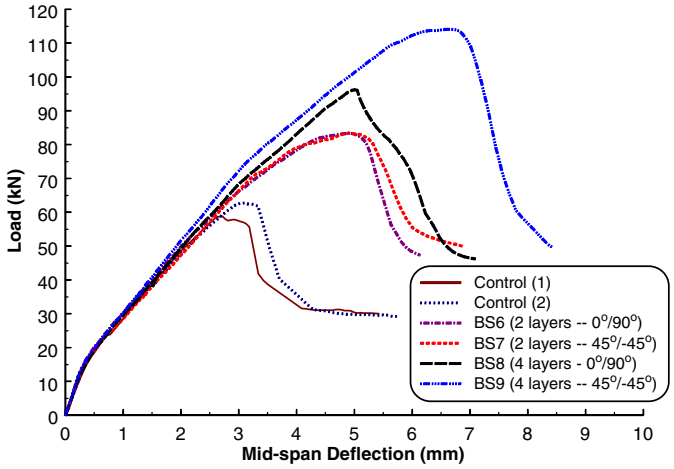

Fig. 7. Load-deflection curves for beams with polymer-modified cementitious mortar

in compression zone as seen in Fig. 8. The average ultimate load for the two beams was 60.8 kN. Similar shear failure was also observed for all strengthened beams BS2 to BS9 as shown in Fig. 8. Even though TRM material used in this study has low bond strength with concrete, bond failure was not evident in the experiments as the induced shear stresses were not enough to mobilize the debonding failure. As a result, TRM layers were generally effective in enhancing the shear capacity of the test beams as gains in ultimate shear resistance ranged from 36–88% as shown in Table 6. The maximum loads in specimens BS2, BS3, BS6, and BS7 were 82.66 kN, 83.51 kN, 83.38 kN, and 83.38 kN, respectively, which are nearly the same. This brings about the conclusion that textile orientation and type of mortar used were not influencing parameters for specimens with two layers of TRM on each side. The maximum load in beams BS4 and BS5 was 88.74 kN and 92.53 kN, respectively. Since both the loads are almost same, it signifies that the textile orientation has little effect on the shear enhancement of beams with four layers of TRM on each side and bonded with cementitious mortar. However, beams BS8 and BS9 failed at maximum loads of 96.26 kN and 114.1 kN, respectively. For the beams strengthened with four layers of TRM on each side and bonded with polymer-modified mortar, the $45°/-45°$ textile orientation showed better shear resistance than that of the $0°/90°$ orientation. In addition, for the beams strengthened with four layers of TRM, polymer-modified mortar was more effective than cementitious mortar in terms of enhancing the shear strength. This demonstrates that the effect of textile orientation and mortar type was insignificant when two layers of TRM were used but more apparent for the beams strengthened with four layers of TRM. The shear strength provided by the TRM system can be attributed to the contribution from textile fiber and the mortar. As the number of TRM layers increases, the effect of textile orientation on the shear strength provided by the textile fiber is enhanced. Similarly for the case of mortar type, as the number of TRM layers increases, the mortar thickness increases and the effect of mortar type on the shear strength provided by the mortar is improved. In addition to the mortar thickness, the shear strength contributed by the mortar is also related to its compressive strength. In this case, since the compressive strength of polymer-modified cementitious mortar is higher than that of cementitious mortar, it was found to be more effective for four layers of TRM.

Table 6. Additional Specimens Considered for the Numerical Study

Specimen identification	Type of strengthening	Number of layers on each side	Fiber orientation within shear-span (°)	Number of repetitions
BS10	TRM (polymer-modified cementitious mortar)	8	0/90	1
BS11	TRM (polymer-modified cementitious mortar)	12	0/90	1
BS12	CFRP sheet	1	90	1

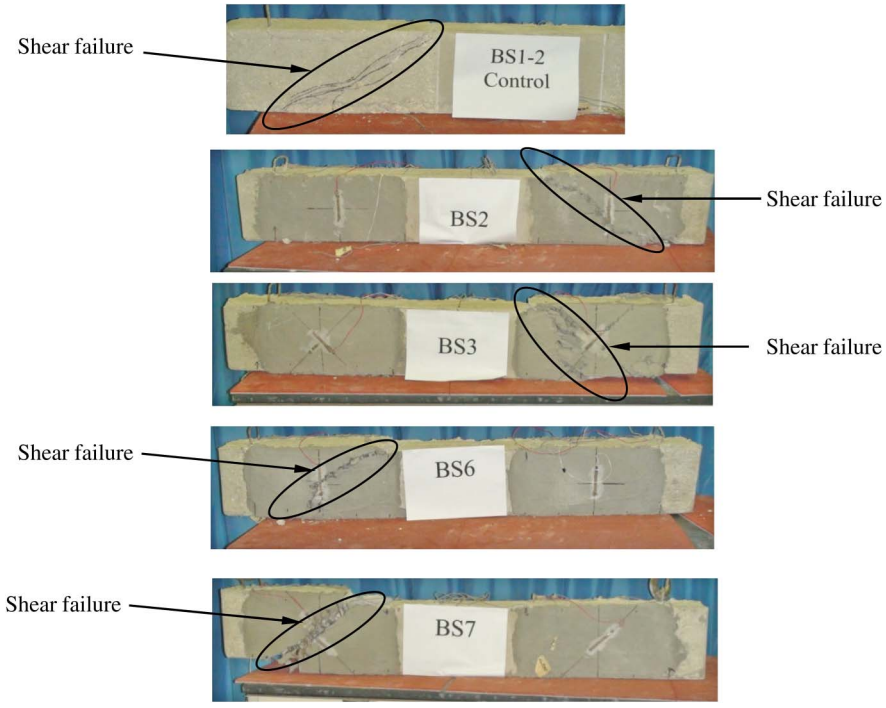

Fig. 8. Mode of failure for representative samples of test beams

Finite Element Modeling

Finite element (FE) modeling of the TRM-strengthened beams was carried out so as to validate the adopted numerical modeling techniques for TRM along with the material model that can be used for modeling the textile-reinforced mortar. LS-DYNA (LSTC 2007), a general-purpose FE program, was employed for the numerical simulation of the TRM-strengthened beams under four-point bending tests. The 3-D finite element model was developed using a general-purpose preprocessor FEMB. Only half of the beam was modeled accounting for its symmetry. Two cases were considered for the FE analysis of strengthened beams. The first case incorporated the modeling of mortar; whereas, the second case omitted the mortar and only the textile was modeled to analyze the importance of modeling mortar for the numerical analysis results.

As seen from the experimental results, four layers of TRM material used in the study were insufficient to shift the shear failure toward a flexural failure in the shear deficient beams. Since it is impractical to use more than four layers in the experimental part, the effect of increasing the number of layers was studied in the numerical part. Finite element analysis was carried out for all the beam samples studied in the experimental part and three other cases were also considered in the numerical study. BS10 and BS11 specimen identifications, correspond to the two new cases which incorporate 8 and 12 textile layers per each side of the beam bonded with polymer-modified cementitious mortar. For the FE analysis of beams strengthened with 8 and 12 layers, only the polymer-modified cementitious mortar was considered as the experimental results depict its performance to be better than the cementitious mortar. Another specimen BS12, strengthened in shear with a single layer of CFRP sheet per each side of the beam, was also modeled to compare with results from the specimen BS11. The selection of specimen BS12 was considered to provide the same shear enhancement as 12 layers of TRM composite used in this study as calculated from the design guidelines in ACI 440.2R-08 (ACI 2008). Fig. 9 shows the schematic detail for beam specimen BS12 as strengthened with a single layer of CFRP sheet. Table 6 enlists the details of the considered parameters for the analysis of BS10, BS11, and BS12.

Model Geometry

To mimic the real behavior of tested RC beams, it is imperative that the concrete volume be modeled using solid elements. For this rea-

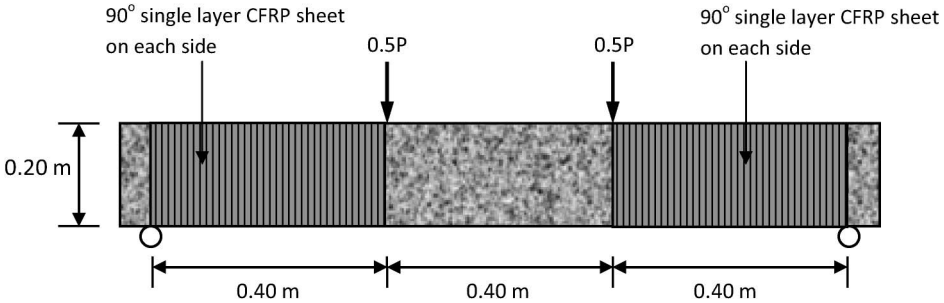

Fig. 9. Details of specimen BS12 strengthened with CFRP sheet (numerical study only)

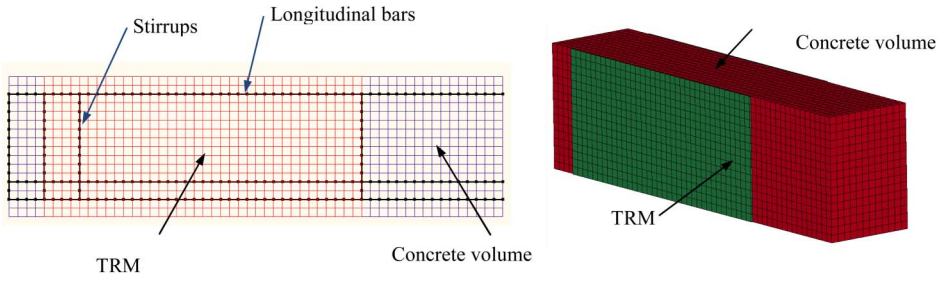

Fig. 10. Finite element mesh in FEMB software showing the modeled components

son, 8-node reduced integration solid elements were used to model the concrete. The longitudinal reinforcing bars and the transverse ties were modeled using 2-node Hughes Lui beam elements. The basalt-based textile and the carbon/epoxy composite were modeled using 4-node shell elements. The Belytschko-Tsay (Belytschko and Tsay 1981) element formulation was used for all shell elements. The textile, arranged in two orthogonal directions, was smeared into orthotropic material with an equivalent thickness of 0.064 mm per layer. Finally, 8-node solid elements were used to model the mortar.

The concrete volume was modeled by cube elements of 13 mm in size. Numerical convergence study showed that further decrease in the mesh size has little effect on the numerical results but leads to the risk of computer memory overflow and substantially increases the computing time. To achieve maximum computing efficiency and thereby reduce the run-time, it was decided to use 13-mm cubes to model the concrete. Fig. 10 shows the typical mesh of the TRM-strengthened beam which consists of 10,751 solid concrete elements, 485 beam elements for the reinforcing bars, 1,152 textile shell elements, and 1,152 solid mortar elements to give a total of 13,540 elements.

Material Modeling

The material model type 159, MAT_CSCM_CONCRETE, was employed to model both the concrete for the beam and the mortar for the TRM. This is a smooth or continuous cap model available in LS-DYNA for solid elements, with a smooth intersection between the shear yield surface and the hardening cap as shown in Fig. 11. In this model, the initial damage surface coincides with the yield surface. Fig. 11 shows the general shape of concrete model yield surface in two dimensions. The yield surface is formulated in terms of three stress invariants because an isotropic material has three independent stress invariants. The model uses J_1 = first invariant of the stress tensor, J_2' = second invariant of the deviatoric stress tensor, and J_3' = third invariant of the deviatoric stress tensor. The invariants are defined in terms of the deviatoric stress tensor, S_{ij} and pressure, P as follows:

$$J_1 = 3P \tag{1}$$

$$J_2' = \frac{1}{2} S_{ij} S_{ij} \tag{2}$$

$$J_3' = \frac{1}{3} S_{ij} S_{jk} S_{ki} \tag{3}$$

The three-invariant yield function is on the basis of these three invariants and the cap hardening parameter K as shown in Eq. (4).

$$f(J_1, J_2', J_3', K) = J_2' - R^2 F_f^2 F_c \tag{4}$$

Here F_f = shear failure surface; F_c = hardening cap; and R = Rubin three-invariant reduction factor. The cap hardening parameter, K, is the value of the pressure invariant at the intersection of the cap and shear surfaces. For the shear failure surface, the strength of concrete is modeled by the shear surface in the tensile and low confining pressure regimes. The shear surface F_f is defined along the compression meridian as shown in Eq. (5).

$$F_f(J_1) = \alpha - \lambda \exp^{-\beta J_1} + \theta J_1 \tag{5}$$

Here the values of α, β, λ, θ are selected by fitting the model surface to strength measurements from tests conducted on plain concrete cylinders.

The strength of concrete is modeled by a combination of the cap and shear surfaces in the low to high confining pressure regimes. More importantly, the cap is used to model plastic volume change related to pore collapse (although the pores are not explicitly modeled). The initial location of the cap determines the onset of plasticity in isotropic compression and uniaxial strain. The elliptical shape of the cap allows the onset for isotropic compression to be greater than the onset for uniaxial strain, in agreement with shear enhanced compaction data. Without ellipticity, a "flat" cap would produce identical onsets. The motion of the cap determines the shape (hardening) of the pressure-volumetric strain curves via fits with data. Without cap motion, the pressure-volumetric strain curves would be perfectly plastic. Rate effects are modeled with viscoplasticity. More details of this material model can be found in references (Murray 2007; Murray et al. 2007).

For modeling the steel reinforcement, material model type 24, MAT_PIECEWISE_ LINEAR_PLASTICITY, was used. This material is suited to model elastoplastic materials with an arbitrary stress versus strain curve and an arbitrary strain rate dependency. It

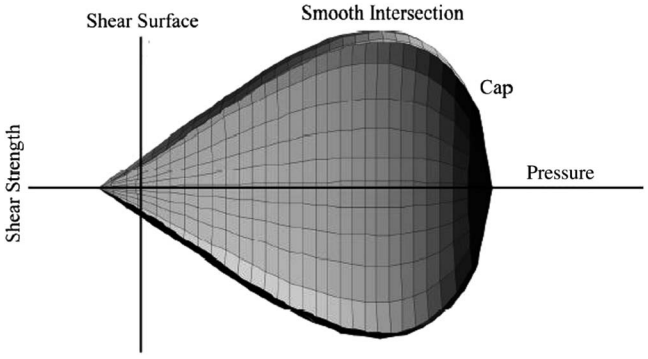

Fig. 11. General shape of the concrete model yield surface in two dimensions

is available for beam, shell, and solid elements. To model the textile material and the CFRP sheets, the material model type MAT_022, MAT_COMPOSITE_DAMAGE was employed. An orthotropic material with optional brittle failure can be defined using this material card. Three failure criteria are possible for this card. The part composite card was used to input the textile and fiber properties. This card provides a simplified method of defining a composite material model for shell elements that eliminates the need for user defined integration points and part identifications for each composite layer. It also allows the input of material identification, composite thickness, and material orientation for each of the composite layers. A summary of the material properties used in this study is presented in Table 7.

Erosion

The erosion option provides a way of including failure to the material models. This is not a material or physics-based property; however, it lends a great means to imitate concrete spalling phenomena and produce graphical plots which are more realistic representations of the actual events. By activating this feature, the eroded solid element is physically separated from the rest of the mesh. Material failure was simulated by element erosion at a specific plastic strain; thus, whenever an element reaches this critical value, it is removed from the computation. This erosion model represents a numerical remedy to distortion, which can cause excessive and unrealistic deformation of the mesh. In this study, elements of concrete and mortar were allowed to erode when the maximum principal strain reached 0.05 (Murray et al. 2007).

Boundary Conditions

Only half of the beam was modeled in LS-DYNA taking into account the symmetry of the beam specimens. A node set was created which consisted of nodes at support location of the beam which had to be restricted for the displacement in the vertical direction. This translates as a roller support near the beam end. Symmetric boundary conditions were applied for the nodes in elements for the plane representing the continuation of the beam in reality. This included restriction of displacement in the corresponding horizontal direction and the rotation about the z-axis for those nodes. Since the loading was displacement controlled, another node set was created which comprised of nodes along the loading plane which were controlled to have the same vertical displacement throughout the duration of the test.

Loading Strategy

LS-DYNA uses explicit time integration algorithms for solving the problems, which are less sensitive to machine precision than other finite element solution methods. The load application process in LS-DYNA is time-history dependent. Since the testing procedure involved displacement controlled static loading, the inertia effects were removed from the dynamic equation by assigning a constant velocity to the displacement controlled node set. This will lead to zero acceleration and, hence, zero inertia force. The rate of change of displacement was defined as 1 mm/ min to match with the experimental loading.

Table 7. Material Properties Used in the FE Modeling

Concrete	
Material model	MAT_CSCM_CONCRETE
Density (kg/m^3)	2,320
Uni-axial compressive strength (MPa)	20
Maximum aggregate size (mm)	10
Mortar	
Material model	MAT_CSCM_CONCRETE
Density (kg/m^3)	1,960
Uni-axial compressive strength (MPa)	• 23.9 (cementitious mortar) • 56.4 (polymer-modified cementitious mortar)
Maximum aggregate size (mm)	5
Longitudinal reinforcement	
Material model	MAT_PIECEWISE_LINEAR_PLASTICITY
Density (kg/m^3)	7,850
Modulus of elasticity (MPa)	200,000
Poisson's ratio	0.30
Yield stress (MPa)	575
Plastic strain to failure	0.077125
Transverse reinforcement	
Material model	MAT_PIECEWISE_LINEAR_PLASTICITY
Density (kg/m^3)	7,850
Modulus of elasticity (MPa)	200,000
Poisson's ratio	0.30
Yield stress (MPa)	240
Failure strain	0.19825
Basalt-based textile	
Material model	MAT_COMPOSITE_DAMAGE
Density (kg/m^3)	1,740
Young's modulus in the longitudinal direction (MPa)	31,940
Young's modulus in the transverse direction (MPa)	31,940
Poisson's ratio	0.22
Shear modulus (MPa)	13,090
Longitudinal tensile strength (MPa)	623
Transverse tensile strength (MPa)	623
CFRP sheet	
Material model	MAT_COMPOSITE_DAMAGE
Thickness of each layer (mm)	1.0
Young's modulus in the longitudinal direction (MPa)	77,300
Young's modulus in the transverse direction (MPa)	3,380
Longitudinal tensile strength (MPa)	846
Transverse tensile strength (MPa)	40.6

Finite Element Results and Discussion

Modes of Failure

Figs. 12–14 depict the modes of failure for representative beam specimens as observed from the FE analysis postprocessing software. The failure modes in the figures are on the basis of contours of midsurface maximum principal strains for models which incorporated the mortar used for binding the textile material. From the analysis, it was found that the control beam as well as all beam specimens incorporating 2–4 layers of TRM strengthening (BS2, BS3, BS4, BS5, BS6, BS7, BS8, and BS9) failed in shear in agreement with the experimental results. Figs. 12 and 13 show this failure for the control as well as beam specimens BS2 and BS9,

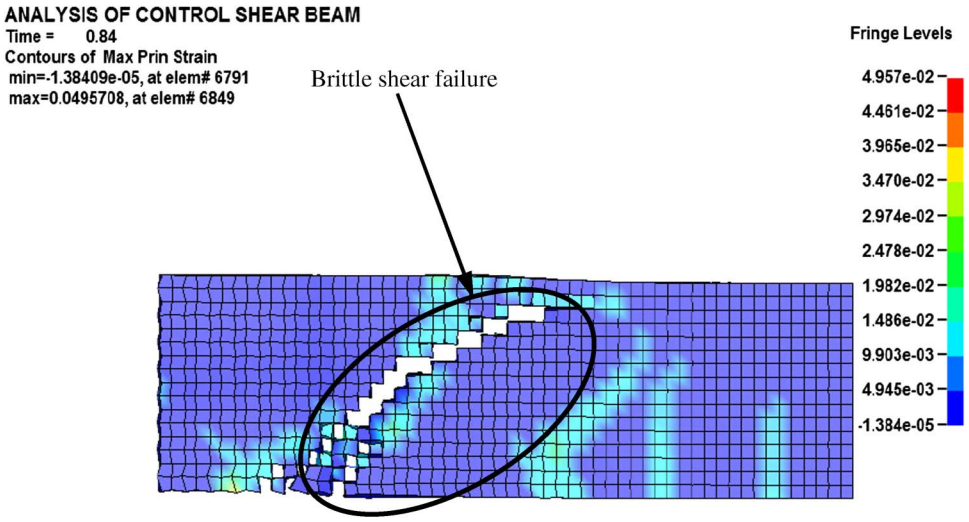

Fig. 12. Contours of maximum principal strain in the concrete volume for control beams

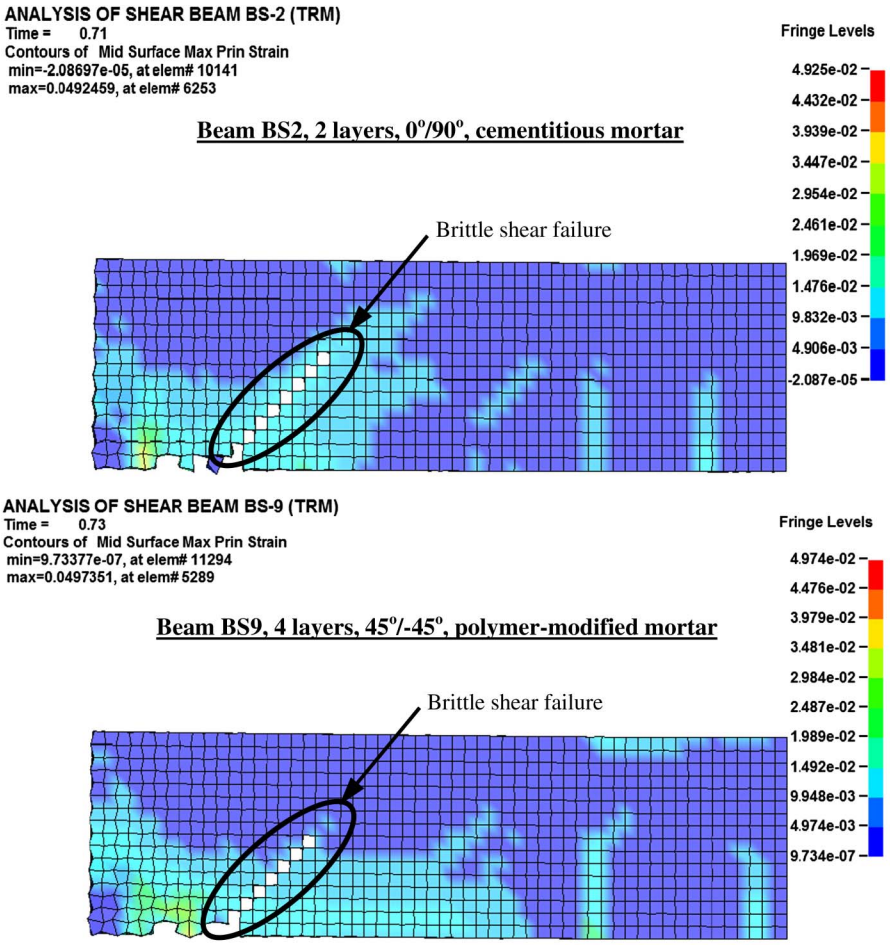

Fig. 13. Contours of maximum principal strain in the concrete volume for representative cases of TRM-strengthened beams

respectively. As presented in Fig. 14, specimen BS10 which was considered in the FE analysis only also failed in shear which explains that even eight layers of the textile material used in this study would not be enough to shift the shear failure to a flexural one. However, as seen from Fig. 14, specimen BS11 (with 12 layers of TRM each side), the failure mode incorporates flexural cracks and evidently a flexural failure. Fig. 14 incorporates the failure mode, as per the analysis, for the CFRP-strengthened specimen BS12 which failed in flexure as evident from the flexural cracks in the maximum moment region.

Load-Deflection Curves

A comparison was made between the load-deflection curves obtained from the experimental and the numerical studies for all

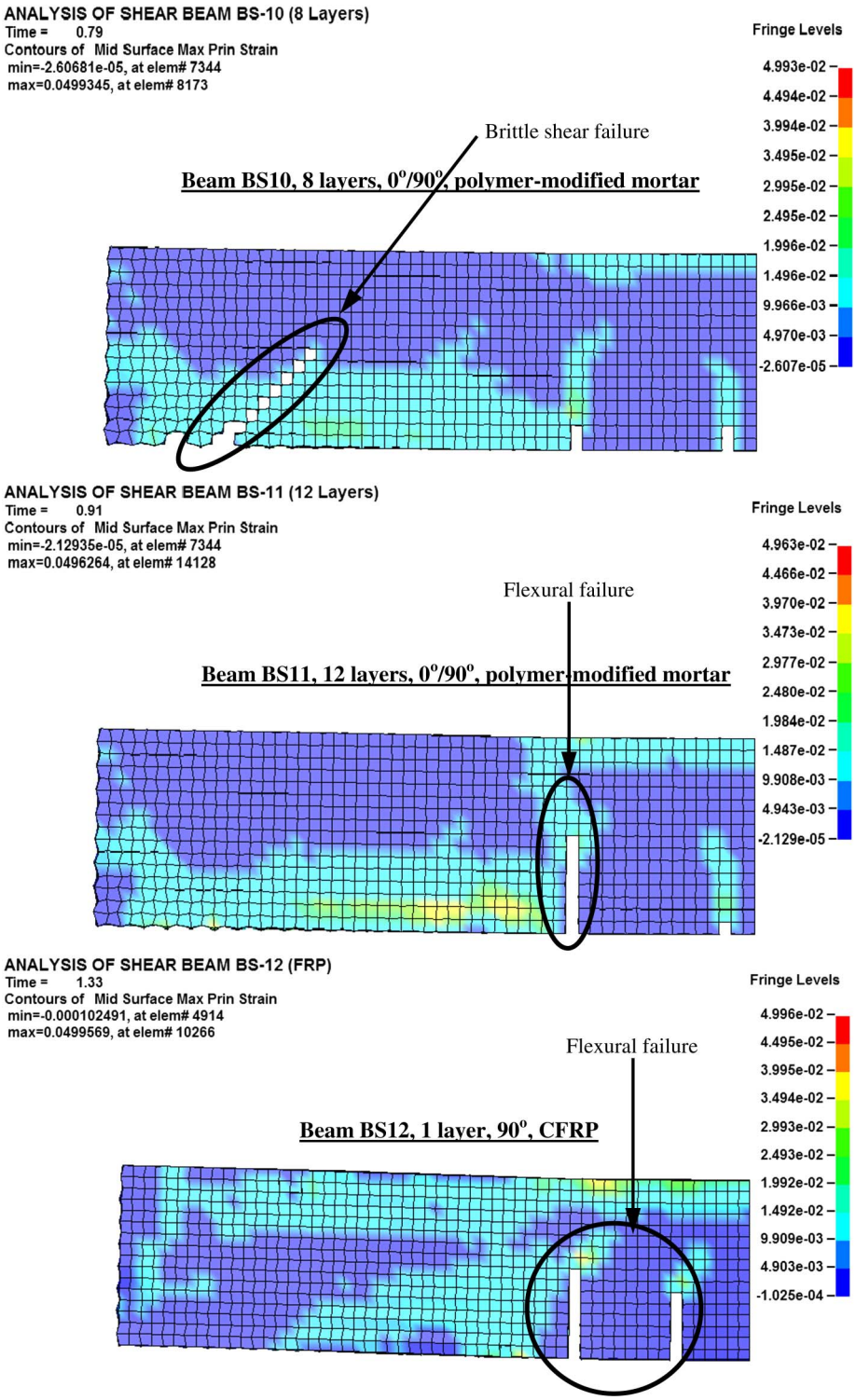

Fig. 14. Contours of maximum principal strain in the concrete volume for beams BS10, BS11, and BS12

the beam specimens. Figs. 15–17 depict this comparison. The results from the numerical model which did not include the mortar were also included for comparison. As seen from the figures, the experimental load-deflection curves showed good agreement especially for the ultimate load, carrying capacity compared with the FE analysis of the control beam as well as TRM-strengthened beams with mortar modeled. For most of the beams, the ultimate load-carrying capacity and the midspan deflection in the plastic region were only slightly higher for the numerical results. Table 8 enlists the comparison details. As seen in Table 8, a maximum deviation of 8% was found for the numerical results for the ultimate load-carrying capacity of the beams and 27% was found for the midspan deflection compared with the experimental results. The overestimation of deflections in the FE results could be attributed to a few reasons. Owing to the symmetry of the beam, only half of the beam was modeled in the FE study. As seen in Fig. 8, for all specimens in the experimental study, the shear failure was only recorded in one of the shear spans of the beam depending on the material properties.

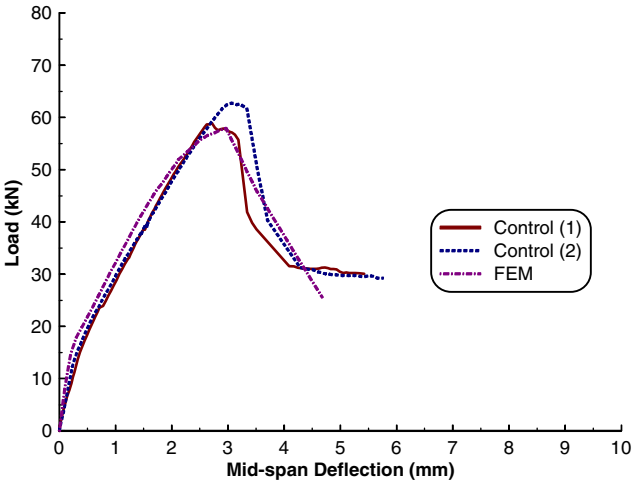

Fig. 15. Load-deflection comparison for control beams

However, in the FE study, the shear failure would ideally be representative on both the shear spans of the beam. Accordingly, two main shear cracks would be observed in the FE analysis results of the beam specimen compared with the main single crack detected in the experimental testing. Hence, the midspan deflection recorded at ultimate load in the FE study could be slightly overestimated compared with the experimental results.

The stiffness of the beam specimens was also predicted efficiently by the FE models in comparison with the experimental results. The figures also show that the FE models were successful in imitating the softening behavior which demonstrates the accuracy of the material model. It was found from this comparison that the model incorporating the mortar (TRM) illustrates better behavior compared to the model which excludes mortar modeling. This was true especially as the number of TRM layers increased and for the case of polymer-modified cementitious mortar specimens. Since, with the increase in the number of TRM layers, the thickness of mortar increases, thereby the contribution of mortar toward the shear strength also increases. Also, for the case of polymer-modified cementitious mortar specimens (BS8 and BS9), as seen from Fig. 17, the behavior for the model which incorporated mortar was better compared with the model with textile only. It could be attributed to the fact that the compressive strength of this type of mortar was higher which indicates the need to incorporate mortar modeling in the FE analysis.

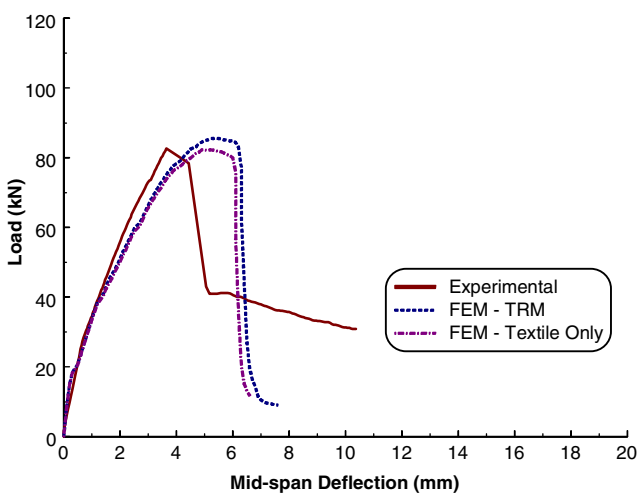

(a) Specimen BS2

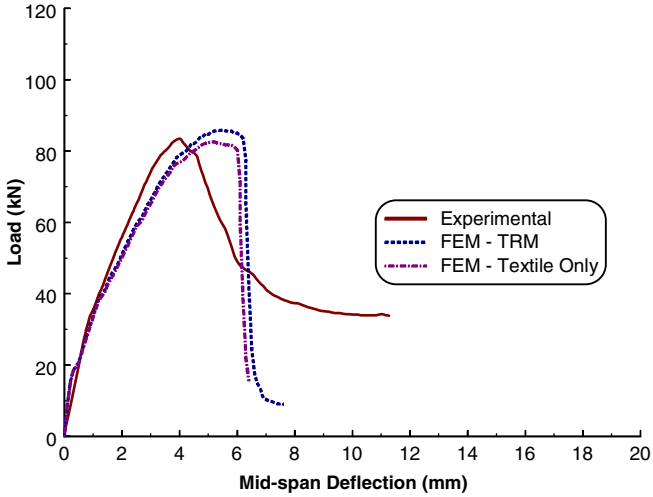

(b) Specimen BS3

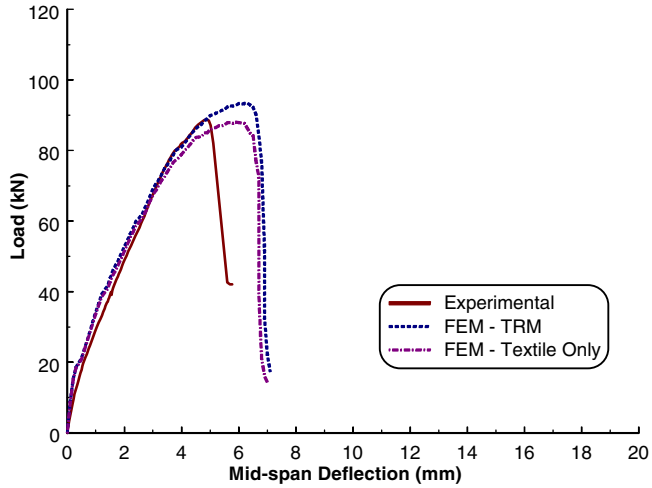

(c) Specimen BS4

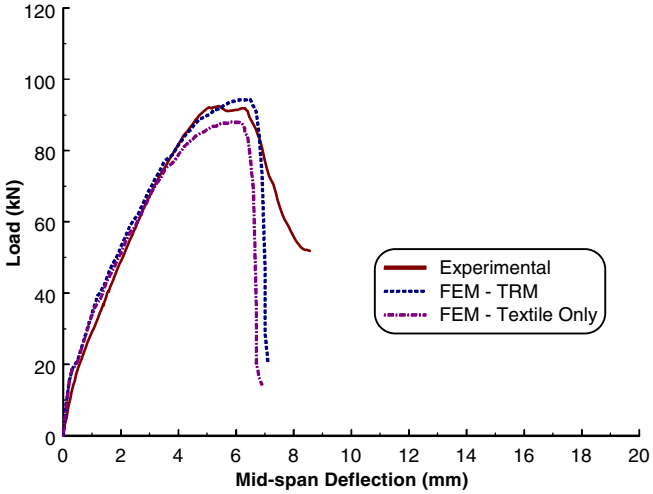

(d) Specimen BS5

Fig. 16. Load-deflection comparison for beams with cementitious mortar

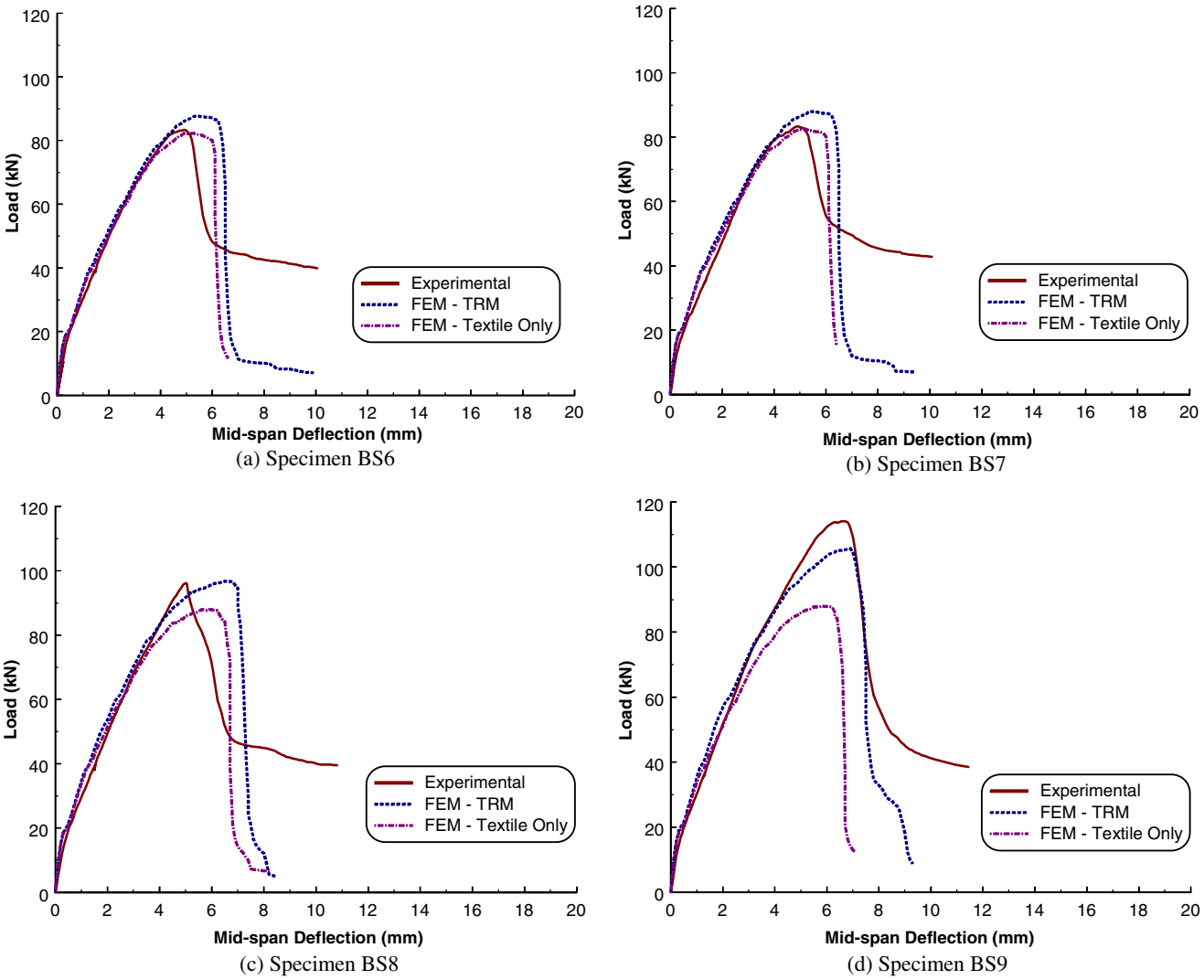

Fig. 17. Load-deflection comparison for beams with polymer-modified cementitious mortar

Table 8. Summary of Results for All Beams

Specimen identification	Ultimate load (P_u) (kN)			Midspan deflection at ultimate load (mm)			Percent gain in shear capacity		Mode of failure
	EXP	NUM	EXP/NUM	EXP	NUM	EXP/NUM	EXP	NUM	
BS1-1	58.94	57.9	1.02	2.715	2.95	0.92	—	—	Shear failure
BS1-2	62.73	57.9	1.08	3.065	2.95	1.04	—	—	Shear failure
BS2	82.66	85.6	0.97	3.99	5.4	0.74	35.9	47.8	Shear failure
BS3	83.51	85.9	0.97	4.02	5.5	0.73	37.3	47.8	Shear failure
BS4	88.74	93.4	0.95	4.895	6.3	0.78	45.9	61.3	Shear failure
BS5	92.53	94.3	0.98	5.405	6.5	0.83	52.1	62.9	Shear failure
BS6	83.38	87.7	0.95	4.9	5.4	0.91	37.1	51.5	Shear failure
BS7	83.38	88	0.95	4.95	5.4	0.92	37.1	52	Shear failure
BS8	96.26	96.8	0.99	5.005	6.5	0.77	58.2	67.1	Shear failure
BS9	114.1	105.7	1.08	6.64	6.9	0.96	87.6	82.5	Shear failure
BS10	—	117.5		—	7.9		—	102.9	Shear failure
BS11	—	123.9		—	9.4		—	114	Flexural failure
BS12	—	126		—	12		—	117.6	Flexural failure

Fig. 18 shows the load-deflection curves for the specimens BS10, BS11, and BS12 obtained on the basis of the results from the FE analysis. The predicted ultimate load capacity for the beam specimens BS10, BS11, and BS12 was 117.5, 123.9, and 126 kN, respectively, and the midspan deflection at the ultimate load for the specimens was 7.9, 9.4, and 12 mm, respectively. From the load-deflection behavior of the specimen BS11 and as a result of 12 TRM layers, the ductility of the beam system was slightly

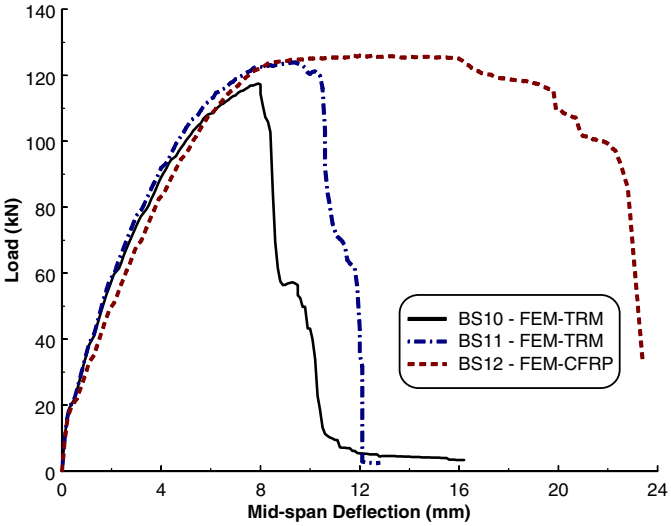

Fig. 18. Load-deflection curve for beams BS10, BS11, and BS12

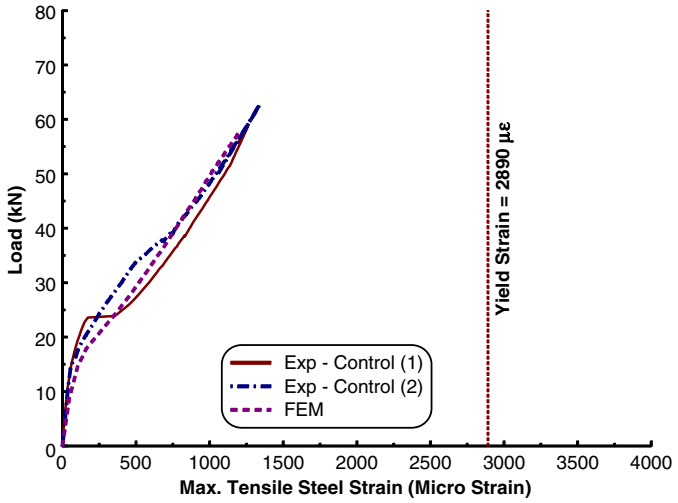

Fig. 19. Load versus longitudinal steel strain comparison for control beams

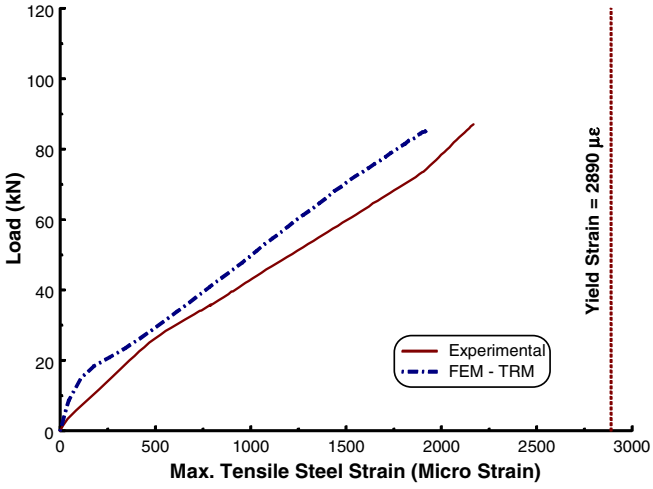

(a) Specimen BS2

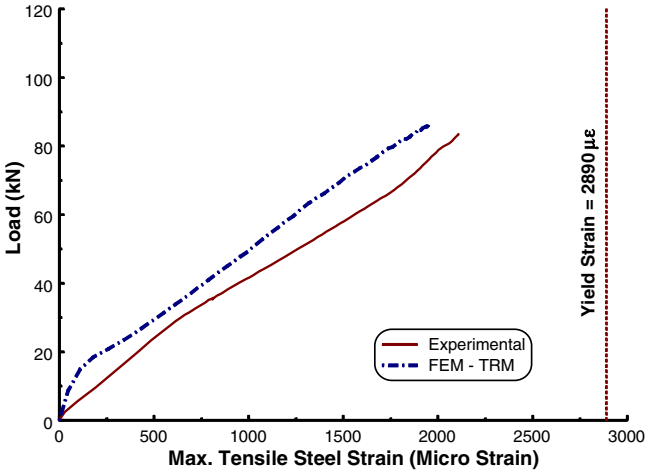

(b) Specimen BS3

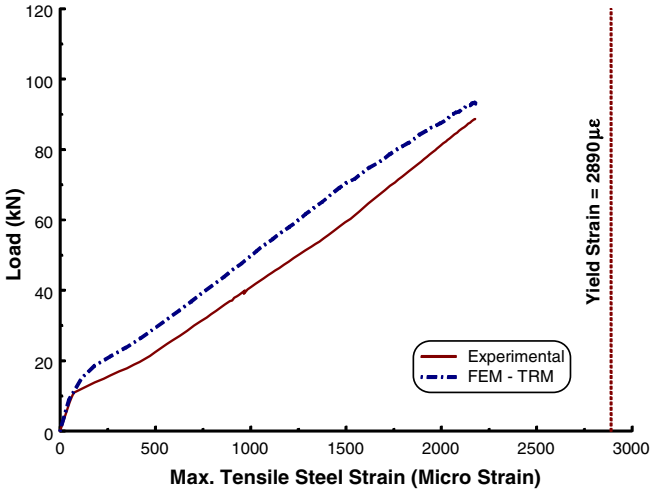

(c) Specimen BS4

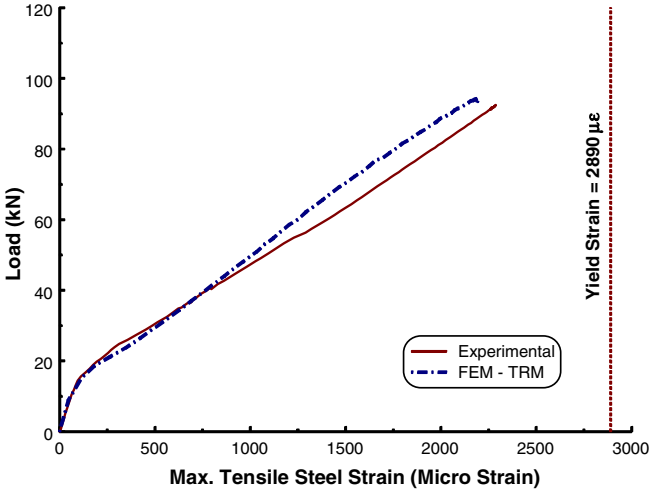

(d) Specimen BS5

Fig. 20. Load versus longitudinal steel strain comparison for beams with cementitious mortar

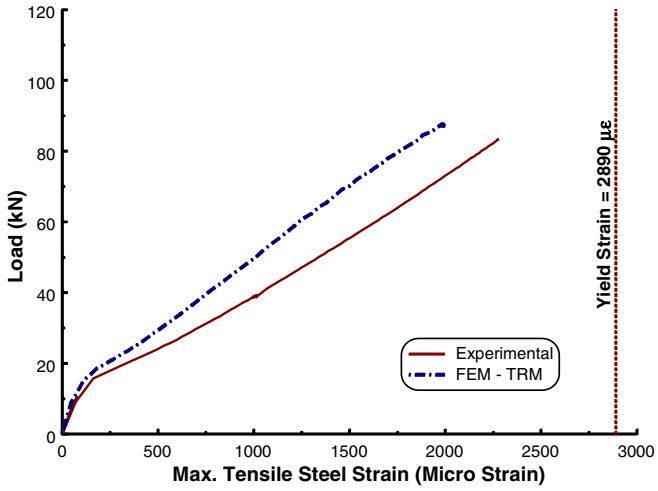

(a) Specimen BS6

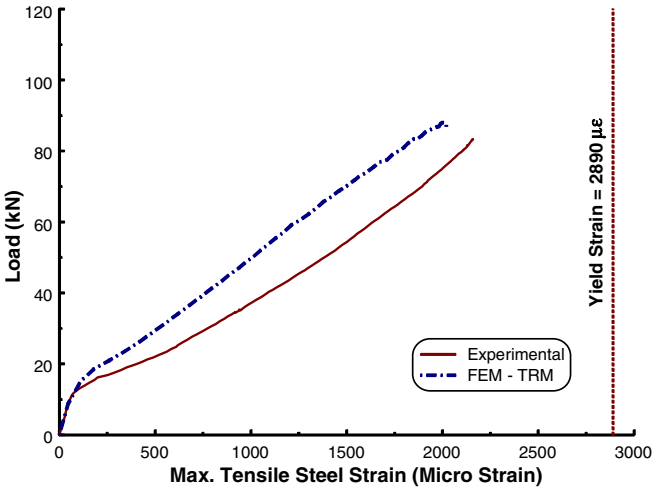

(b) Specimen BS7

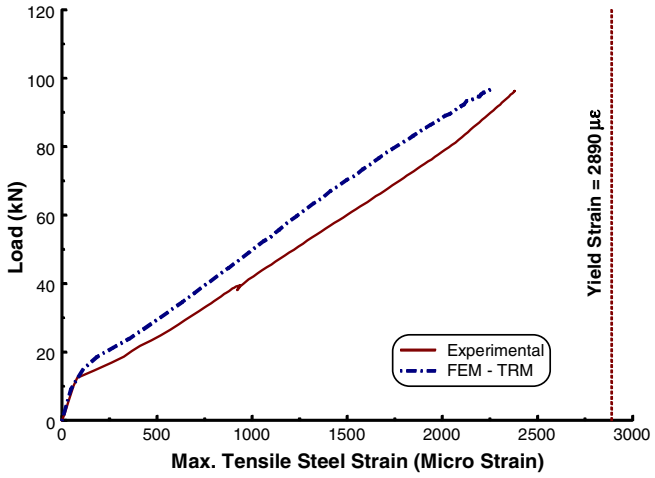

(c) Specimen BS8

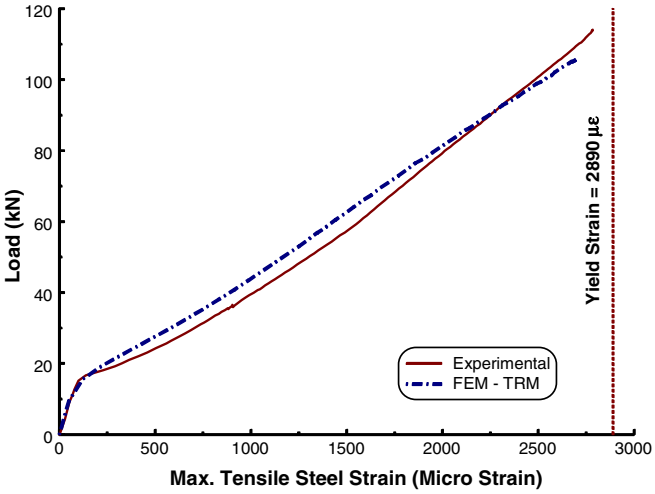

(d) Specimen BS9

Fig. 21. Load versus longitudinal steel strain comparison for beams with polymer-modified cementitious mortar

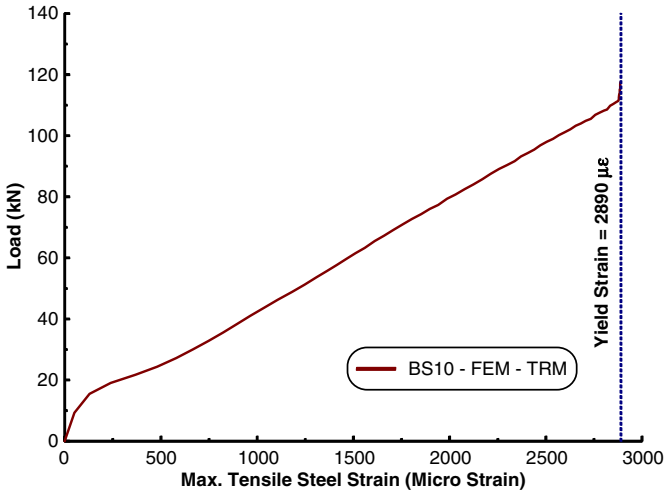

Fig. 22. Load versus longitudinal steel strain for beam BS10

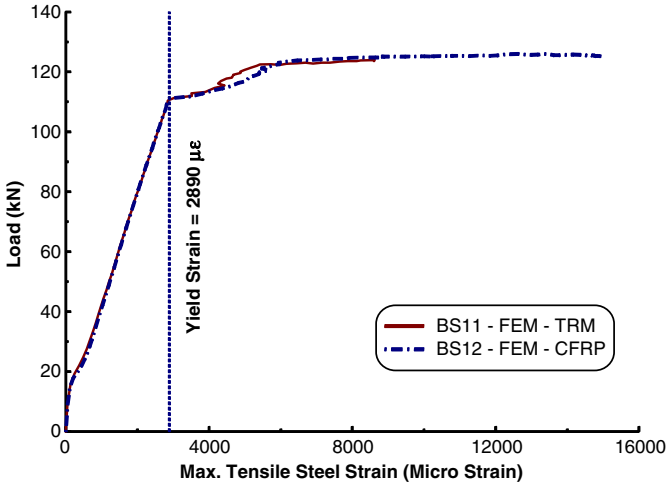

Fig. 23. Load versus longitudinal steel strain for beams BS11 and BS12

improved. However, for specimen BS12 strengthened with CFRP sheet, the ductility of the beam was greatly enhanced compared with the TRM system.

Strain Gauge Results

The maximum tensile strain in the longitudinal steel obtained from the postprocessing software of LS-DYNA for all the beams specimens was compared with the experimental steel strains obtained using the strain gauges. Figs. 19–21 depict this comparison. From the figures it can be inferred that, for all experimental specimen ranging from BS2 to BS9 the strain in the longitudinal steel did not reach the yield strain value which would trigger a flexural failure, and therefore, a shear failure was noticed in all the beams. This behavior is clearly visible from the numerical results also and the curves show good agreement between the experimental and the numerical results. For beam BS10, the steel strain was slightly less than the yield value as shown in Fig. 22. As seen in Fig. 23 for the specimens BS11 and BS12, the numerical modeling results predict that the strain in the steel would exceed the yield strain values thereby indicating a shift toward flexural failure as a result of increasing the number of TRM layers for shear strengthening and the enhanced shear strength contributed by the CFRP sheet.

Conclusions

On the basis of experimental and numerical results presented in this paper, the following conclusions can be drawn.

1. The basalt textile-reinforced mortar layers provided substantial gain in the shear capacity of reinforced concrete beams ranging from 36–88%. As anticipated, the shear resistance increased as the number of TRM layers increased from two to four per side.
2. Because of the weakness of the basalt textile used in this research, the number of layers used (two and four layers per side) did not prohibit the sudden shear failure, which could have been avoided either by selecting a stronger textile or by increasing the number of TRM layers. However, the brittle shear failure of strengthened beams means that all TRM layers were fully mobilized and if more layers were added, flexural failure would have been activated.
3. With four layers each side of TRM, the $45°/-45°$ textile showed better shear resistance than that with the $0°/90°$ orientation and the polymer-modified mortar was more effective than the cementitious mortar in terms of enhancing the shear strength.
4. An FE analysis was carried out which incorporated the geometric and material modeling for the TRM beam system. Comparison of the FE analysis results with the experimental results confirmed that the proposed numerical approach is appropriate for estimating the ultimate load-carrying capacity of both the unstrengthened and TRM-strengthened concrete beams. This will thereby indicate the validity of the numerical modeling procedures, which may be used for conducting future research in the area of TRM-upgraded concrete elements.
5. A comparison between TRM and CFRP systems in the numerical part indicated that on the basis of the textile fibers used in this study, 12 layers of TRM would be required to provide the same shear enhancement as that of a single layer of CFRP laminate. From this study, it is concluded that the TRM system would be a promising solution for shear strengthening of RC beams provided textile material of higher strength is used. The basalt-based textile material used in the present study might be uneconomical for shear enhancement of RC beams.

Acknowledgments

The authors gratefully acknowledge the support provided by the Specialty Units for Safety and Preservation of Structures and the MMB Chair for Research and Studies in Strengthening and Rehabilitation of Structures at the College of Engineering, King Saud University.

References

American Concrete Institute (ACI). (2008). "Guide for the design and construction of externally bonded FRP systems for strengthening concrete structures." *ACI 440.2R-08*, American Concrete Institute, Farmington Hills, MI.

American Society for Testing and Materials (ASTM). (1985). "Method of test for tensile strength of hydraulic cement mortars." *ASTM C190*, American Society for Testing and Materials, West Conshohocken, PA.

American Society for Testing and Materials (ASTM). (2008). "Standard test method for compressive strength of hydraulic cement mortars (using 2-in. or [50-mm] cube specimens)." *ASTM C109/C109M*, American Society for Testing and Materials, West Conshohocken, PA, 10.1520/C0109_C0109M-08.

American Society for Testing and Materials (ASTM). (2009). "Standard test method for pull-off strength of coatings using portable adhesion testers." *ASTM D4541-09e1*, American Society for Testing and Materials, West Conshohocken, PA, 10.1520/D4541-09E01.

American Society for Testing and Materials (ASTM). (2009). "Standard test methods for tension testing of metallic materials." *ASTM E8/E8M*, American Society for Testing and Materials, West Conshohocken, PA, 10.1520/E0008_E0008M-09. 3

American Society for Testing and Materials (ASTM). (2010). "Standard test method for compressive strength of cylindrical concrete specimens." *ASTM C39/C39M*, American Society for Testing and Materials, West Conshohocken, PA, 10.1520/C0039_C0039M-10.

Belytschko, T. B., and Tsay, C. S. (1981). "Explicit algorithms for non-linear dynamics of shells." *AMD, ASME*, 48, 209–231, West Conshohocken, PA, 10.1520/D4541-09E01. 4 5

Bruckner, A., Ortlepp, R., and Curbach, M. (2008). "Anchoring of shear strengthening for *T*-beams made of textile reinforced concrete (TRC)." *J. Mater. and Structures, RILEM*, 41(2), 407–418, .

Curbach, M., and Brueckner, A. (2003). "Textile strukturen zur querkraftverstaerkung von stahlbetonbauteilen." *2nd colloquium on textile reinforced structures*, M. Curbach, ed., Dresden, 347–360 (in German). 6

Curbach, M., and Ortlepp, R. (2003). "Besonderheiten des verbundverhaltens von verstaerkungsschichten aus textilbewehrtem." *2nd colloquium on textile reinforced structures*, M. Curbach, ed., Dresden, 361–374 (in German). 7

Di Ludovico, M., Prota, A., and Manfredi, G. (2010). "Structural upgrade using basalt fibers for concrete confinement." *J. Compos. Constr., ASCE*, 14(5), 541–552.

fib bulletin 14. (2001). "Externally bonded FRP reinforcement for RC structures." *Technical Rep. prepared by the Working Party EBR of Task Group 9.3*, International Federation for Structural Concrete, Lausanne, Switzerland.

Garon, R., Balaguru, P. N., and Toutanji, H. (2001). "Performance of inorganic polymer-fiber composites for strengthening and rehabilitation of concrete beams." *FRPRCS-5 fiber reinforced plastics for reinforced concrete structures*, C. J. Burgoyne, ed., Thomas Telford, London, Vol. 1, 53–62.

Kurtz, S., and Balaguru, P. (2001). "Comparison of inorganic and organic matrices for strengthening of RC beams with carbon sheets." *J. Struct. Eng., ASCE*, 127(1), 35–42.

Larbi, A. S., Contamine, R., Ferrier, E., and Hamelin, P. (2010). "Shear strengthening of RC beams with textile reinforced concrete (TRC) plate." *J. Constr. and Building Mater.*, 24(10), 1928–1936.

Livermore Software Technology Corporation (LSTC). (2007). "LS-DYNA user's keyword manual (nonlinear dynamic analysis of structures in three dimensions) Volume 1." Version 971. 8

Murray, Y. D. (2007). "Users manual for LS-DYNA concrete material model 159." *Rep. No. FHWA-HRT-05-062*, Federal Highway Administration.

Murray, Y. D., Abu-Odeh, A., and Bligh, R. (2007). "Evaluation of concrete material model 159." *Rep. No. FHWA-HRT-05-063*, Federal Highway Administration.

Papanicolaou, C. G., Triantafillou, T. C., Papathanasiou, M., and Karlos, K. (2008). "Textile reinforced mortar (TRM) versus FRP as strengthening material of URM walls: Out-of-plane cyclic loading." *J. Mater. and Structures, RILEM*, 41(1), 143–157.

Toutanji, H., Deng, Y., and Jia, M. (2003). "Fatigue performance of RC beams strengthened with CF sheets bonded by inorganic matrix." *FRPRCS-6 fiber reinforced polymer reinforcement for concrete structures*, K. H. Tan, ed., World Scientific, Vol. 2, 875–884.

Triantafillou, T. C., and Papanicolaou, C. G. (2006). "Shear strengthening of reinforced concrete members with textile reinforced mortar (TRM) jackets." *J. Mater. and Structures, RILEM*, 39(1), 93–103.

Triantafillou, T. C., Papanicolaou, C. G., Zissimopoulos, P., and Laourdekis, T. (2006). "Concrete confinement with textile reinforced mortar (TRM) jackets." *ACI Struct. J.*, 103(1), 28–37.

Wiberg, A. (2003). "Strengthening of concrete beams using cementitious carbon fibre composites." Ph.D. thesis, Royal Institute of Technology, Stockholm.

Wu, H. C., and Sun, P. (2005). "Fiber reinforced cement based composite sheets for structural retrofit." *Proc., Int. Symposium on Bond Behaviour of FRP in Structures (BBFS 2005)*, International Institute for FRP in Construction, Hong Kong.

Wu, H. C., and Teng, J. (2003). "Concrete confined with fiber reinforced cement based thin sheet composites." *FRPRCS-6 fiber reinforced polymer reinforcement for concrete structures*, K. H. Tan, ed., World Scientific, Vol. 1, 591–600.

Queries

1. Textile-Reinforced Mortar (C head), paragraph 3, sentence 2 - "... of the dimensions given in Fig. 4(c) ... " There are only part labels a and b in Fig. 4. Please correct the text.
2. Textile-Reinforced Mortar (C head), paragraph 3, sentence 3 - "... as shown in Fig. 4(d) ... " There are only part labels a and b in Fig. 4. Please correct the text.
3. ASTM 2009 - please indicate a cross reference for this citation in the text or indicate that it should be deleted from the References.
4. Belytschko and Tsay 1981 - a check of online databases revealed possible errors in this reference (published date and DOI number). Please confirm this citation is correct
5. Provide issue.
6. Curbach and Brueckner 2003 - please provide publisher's name.
7. Curbach and Ortlepp 2003 - please provide publisher's name.
8. Livermore Software Technology Corporation 2007 - please provide publisher's name and location.
9. Murray 2007 - please provide publisher's location.
10. Murray et al. 2007 - please provide publisher's location.
11. Toutanji et al. 2003 - please provide publisher's location.
12. Wu and Teng 2003 - please provide publisher's location